Combinatorial Selection Among Geometrical Isomers of Discrete Long-Carbon-Chain Naphthalenediimides Induces Local Order at the Liquid/Solid Interface

Berrocal, Jose Augusto; Heideman, G. Henrieke ; De Waal, Bas F.M.; Meijer, E. W.; Feringa, Ben L.

Published in:
Acs Nano

DOI:
10.1021/acsnano.0c06274

Publication date:
2020

ACS NANO

www.acsnano.org

ARTICLE

Combinatorial Selection Among Geometrical Isomers of Discrete Long-Carbon-Chain Naphthalenediimides Induces Local Order at the Liquid/Solid Interface

José Augusto Berrocal,[†] G. Henrieke Heideman,[†] Bas F. M. de Waal, E. W. Meijer,* and Ben L. Feringa*

Cite This: *ACS Nano* 2020, 14, 13865−13875

Read Online

ACCESS | Metrics & More | Article Recommendations | Supporting Information

ABSTRACT: We report two families of naphthalenediimides (NDIs) symmetrically functionalized with discrete carbon chains comprising up to 55 carbon atoms (C_n-NDI-C_n, n = 39, 44, 50, and 55) and their self-assembly at the 1-phenyloctane/highly oriented pyrolytic graphite interface (1-PO/HOPG interface). The compounds differ by the presence or absence of two or three internal double bonds in the carbon chains (unsaturated and saturated C_n-NDI-C_n, respectively). Combinatorial distributions of geometrical isomers displaying either the *E*- or *Z*-configuration at each double bond are obtained for the unsaturated compounds. Analysis of the self-assembled monolayers of equally long unsaturated and saturated C_n-NDI-C_n by scanning tunneling microscopy (STM) reveal that all C_n-NDI-C_n tend to form lamellar systems featuring alternating areas of aromatic cores and carbon chains. Extended chain lengths are found to significantly increase disorder in the self-assembled monolayers due to misalignments and enhanced strength of interchain interactions. This phenomenon is antagonized by the local order-inducing effect of the internal double bonds: unsaturated C_n-NDI-C_n give qualitatively more ordered self-assembled monolayers compared to their saturated counterparts. The use of combinatorial distributions of unsaturated C_n-NDI-C_n geometrical isomers does not represent a limitation to achieve local order in the self-assembled monolayers. The self-assembly process operates a combinatorial search and selects the geometrical isomer(s) affording the most thermodynamically stable pattern, highlighting the adaptive character of the system. Finally, the antagonistic interplay between the extended carbon chain lengths and the presence of internal double bonds brings to the discovery of the lamellar "phase C" morphology for unsaturated C_n-NDI-C_n with $n \geq 50$.

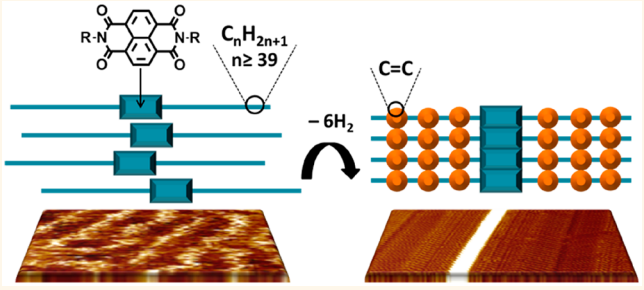

KEYWORDS: *long-chain naphthalenediimides, geometrical isomers, physisorbed monolayers, internal double bonds, long-range order, liquid−solid interface, scanning tunneling microscopy*

The field of self-assembled monolayers on surfaces has become a major research topic in supramolecular chemistry and materials science.[1−6] The possibility to use self-assembled monolayer formation as an attractive alternative to top-down fabrication methods, *e.g.*, for molecular electronics, is a major stimulus to achieve precise control over surface assembly and long-range ordering.[7−9] Besides this well-established research direction, surface-supported supramolecular assemblies have also emerged as attractive platforms to carry out more fundamental studies on multicomponent self-assembly,[10−12] self-assembly in confined spaces (nanocorrals),[13−15] and on-surface chemical reactivity,[16−27] to name but a few. Self-assembled monolayers are typically controlled by a synergistic interplay of substrate−adsorbate, adsorbate−adsorbate, and adsorbate-environment (*i.e.*, solvent, air) non-covalent interactions. Stabilizing substrate−adsorbate interactions are certainly necessary to favor the deposition of molecules.[28,29] In this respect, chemical designs featuring long alkyl chains (up to 18 carbon atoms) are extensively applied on highly oriented pyrolytic graphite (HOPG), thanks to an epitaxial stabilization of 64 meV (1.5 kcal/mol) *per* methylene unit exerted by this substrate.[28,29] Hydrogen bonding

Received: July 27, 2020
Accepted: September 11, 2020
Published: September 11, 2020

Chart 1. Chemical Structures of Unsaturated/Saturated C_n-NDI-C_n and Building Blocks 1−4

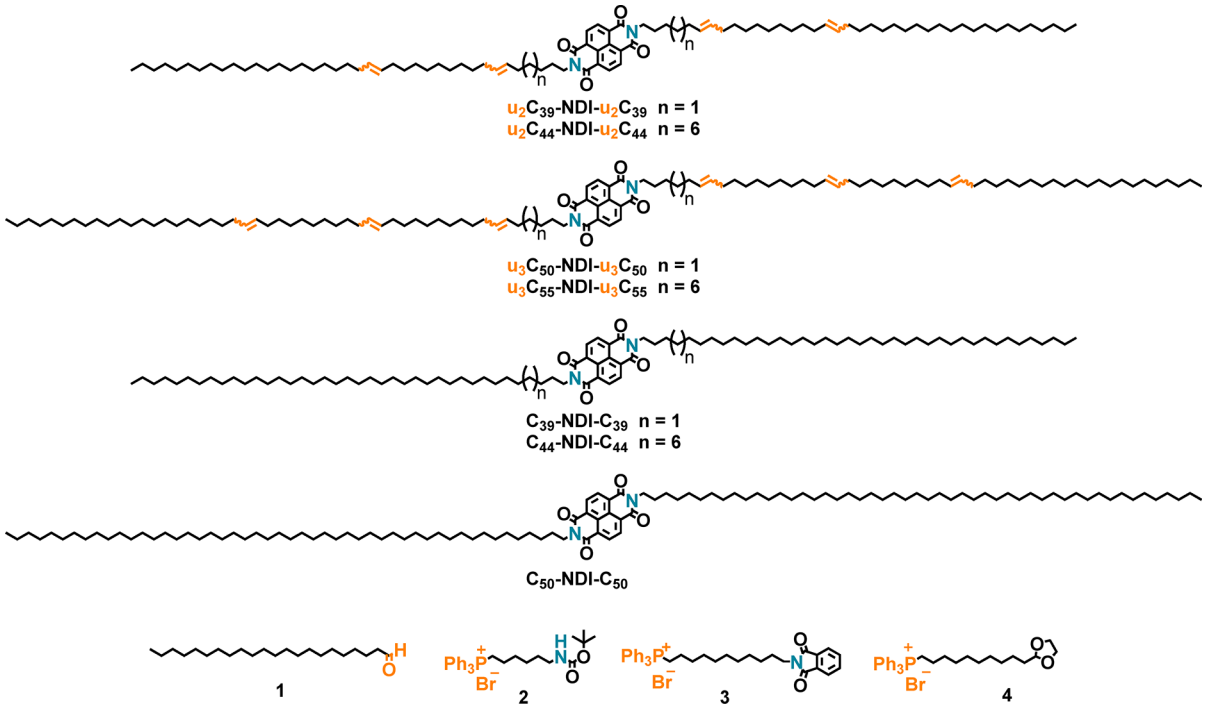

(HB),[30−36] coordination chemistries,[37−39] halogen bonding,[40,41] and van der Waals (vdW) interactions[42−48] have mainly been adopted as adsorbate−adsorbate supramolecular forces, instead.

One of the most intriguing aspects of supramolecular systems at the liquid/solid interface consists of their highly dynamic character, which allows adsorbed compounds and molecules in solution to exchange.[1] Although this aspect can sometimes lead to kinetically trapped states, self-assembled monolayers at the liquid−solid interface typically reach the global minimum energy state.[1] Recent investigations on supramolecular systems at the liquid/solid interface have focused on the interplay between dynamics and thermodynamics.[49−51] For instance, the consequences on self-assembly of the light-triggered *E*−*Z* isomerization of azobenzene moieties in chemical structures featuring two or more of these photoswitches were studied.[49,50] Irradiation with UV or visible light resulted in clear changes in the pattern of the self-assembled monolayers at the liquid/HOPG interface due to *E*−*Z* photoisomerization, as visualized by scanning tunneling microscopy (STM).[49,50] In another study, dynamic combinatorial chemistry[52] (DCC) was coupled to on-surface supramolecular chemistry by STM monitoring of bis-imines at the liquid/HOPG interface.[51] The bis-imines only differed by the length of the *α*,*ω*-diamine building blocks and could interconvert through bistransimination processes on HOPG, which highlighted the adaptive (dynamic) character of these monolayers. The interconversion between bis-imines showed the selection of the component of the dynamic library that presented the thermodynamically most stable physisorption, allowing the whole system to reach thermodynamic minimum.[51] We envisioned that investigating combinatorial libraries of geometrical isomers incapable of interconverting through (photo)chemical reactions, but that still allow for competitive physisorption and pattern formation, could provide additional fundamental knowledge to this recent direction of adaptive or responsive surface-based supramolecular chemistry.

Recently, we have reported on the self-assembly of long aliphatic chain-functionalized naphthalenediimides (**C_n-NDI-C_n** design) at the 1-phenyloctane-HOPG (1-PO/HOPG) interface.[53] The synthesized NDIs featured linear carbon chains consisting of either 28 or 33 carbon atoms (**C_n-NDI-C_n**, $n \leq 33$), which only differed by the presence or absence of internal double bonds (unsaturated/saturated compounds, respectively). The scanning tunneling microscopy (STM) images revealed that all compounds self-assembled into lamellar morphologies with alternating areas of NDI cores (that lay flat and next to each other on the surface) and aliphatic chains (that fill the space in between the aromatic arrangements), in line with previous investigations.[54−56] The unsaturated **C_n-NDI-C_n** consisted of nonseparable mixtures of *ZZ*, *EZ*, and *EE* isomers, but their simultaneous presence did not impede the obtainment of long-range ordered lamellar domains exceeding 15 000 nm^2, which were by far superior to those of the saturated **C_n-NDI-C_n** counterparts in terms of order extent.[53] We proposed the establishment of internal unsaturations as a key structural paradigm for obtaining long-range-ordered assemblies on unconfined surfaces, which is a key challenge in the field.[1]

Building on our discovery of the paramount role of "simple" internal unsaturations in directing self-assembly,[53] we embarked on the study of a library of carbon-chain extended saturated and unsaturated **C_n-NDI-C_n** to elucidate the importance of these so far unrecognized structural parameters. We envisioned that such a study would simultaneously push the limits of self-assembly in terms of chemical structures and stability of the architectures formed, as well as unravel key aspects controlling surface-based supramolecular processes. In this investigation, we address the questions whether the introduction of additional internal double bonds and longer carbon chains in the chemical design of the **C_n-NDI-C_n** system

https://dx.doi.org/10.1021/acsnano.0c06274
ACS Nano 2020, 14, 13865−13875

could play a role in (i) the combinatorial selection among geometrical isomers, and (ii) the extent of order of the self-assembled monolayers. To reach this goal, we synthesized two libraries of $\mathbf{C}_n$-**NDI**-$\mathbf{C}_n$ with linear carbon chains comprising from 39 to 55 carbon atoms (with $39 \leq n \leq 55$, Chart 1), modifying our previous method to obtain discrete oligo-ethylenes.[53] The two $\mathbf{C}_n$-**NDI**-$\mathbf{C}_n$ families differ by the presence/absence of an increasing number of internal double bonds (2 and 3 per chain). The latter, when present, are marked by the letter **u**, followed by the number **2** or **3** as subscript to indicate the total number of double bonds per carbon chain (Chart 1). We show that the combinatorial selection of geometrical isomer(s) occurs only locally, probably due to the tiny energetic differences at stake in such complex systems. Nevertheless, this highlights the dynamic and adaptive character of the $\mathbf{C}_n$-**NDI**-$\mathbf{C}_n$ at the 1-PO/HOPG interface. The discrete extension of the carbon chains in $\mathbf{C}_n$-**NDI**-$\mathbf{C}_n$ is found to significantly decrease the obtainment of long-range order compared to the shorter analogues previously investigated.[53] We attribute this phenomenon to much stronger interchain interactions occurring at the particular chain length regime investigated. These forces locally lead to new lamellar phases in the case of unsaturated $\mathbf{C}_n$-**NDI**-$\mathbf{C}_n$ with $n \geq 50$, in which the typical flat deposition of the NDI cores on HOPG is severely modified.

RESULTS AND DISCUSSION

Synthesis and Characterization. The unsaturated amines ($\mathbf{u}_m\mathbf{C}_n$-$\mathbf{NH}_2$) reported in Chart 2 were the key

Chart 2. Fully Extended Chemical Structures of the Unsaturated Amines ($\mathbf{u}_m\mathbf{C}_n$-$\mathbf{NH}_2$) Featuring 39 ($\mathbf{u}_2\mathbf{C}_{39}$-$\mathbf{NH}_2$), 44 ($\mathbf{u}_2\mathbf{C}_{44}$-$\mathbf{NH}_2$), 50 ($\mathbf{u}_3\mathbf{C}_{50}$-$\mathbf{NH}_2$), and 55 ($\mathbf{u}_3\mathbf{C}_{55}$-$\mathbf{NH}_2$) Carbon Atoms[a]

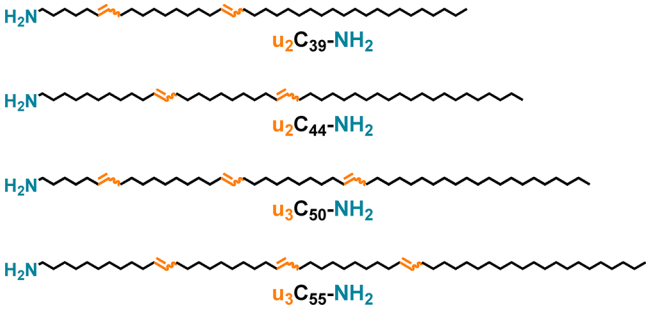

[a]The double bonds are displayed in orange.

synthetic intermediates in the preparation of the $\mathbf{C}_n$-**NDI**-$\mathbf{C}_n$ of Chart 1. The amines were prepared from building blocks **1**–**4** (Chart 1) by iterative Wittig olefination. We highlight the use of building block **4** (see the synthesis in the Supporting Information)—a telechelic molecule featuring a phosphonium salt and an aldehyde moiety masked as ethylene acetal—because this compound allowed us to prepare linear carbon chain lengths comprising more than 33 carbon atoms, overpassing the synthetic limitations of our previous strategy in terms of chain length.[53] The method was inspired by Whiting *et al.*, who prepared model alkane compounds to get insights into the crystallization of polyethylene more than 30 years ago.[57,58]

The synthesis of $\mathbf{u}_m\mathbf{C}_n$-$\mathbf{NH}_2$ started with the Wittig olefination of aldehyde **1** (22-carbon atoms) with **4** (Scheme 1). This reaction allowed us to extend the carbon chain by 11 carbon atoms and install the first double bond along the carbon chain (Scheme 1a). The stereochemistry of the unsaturation was not controlled, but the formation of the *Z*-isomer was favored in view of the conditions of the Wittig olefination applied (non-stabilized phosphorus ylide).[59] The chain extended ethylene acetal intermediate **5** was obtained as an inseparable mixture of *Z* and *E* isomers and was subsequently converted into diethyl acetal **6** by treatment with *p*-toluenesulfonic acid (*p*-TsOH) in a boiling 7:2 ethanol:chloroform mixture, followed by a second reaction with *p*-TsOH in a 1:1 acetone/chloroform mixture at room temperature to afford aldehyde **7** (Scheme 1a).[60] The choice of this two-step deprotection sequence was pivotal to allow an exhaustive **5** → **7** conversion (98% yield), whereas the use of the ethylene acetal moiety provided a reliable and stable protecting group for the more sensitive aldehyde. Iteration of the Wittig olefination sequence from aldehyde **7** and chain extender **4** afforded ethylene acetal **8**, diethyl acetal **9**, and aldehyde **10**, all structures featuring 44 carbon atoms in the main chain (Scheme 1a). Alternatively, aldehydes **7** and **10** were treated with building blocks **2** and **3** under Wittig olefination conditions (Scheme 1b). These reactions further extended the carbon chains by either 6 or 11 carbon atoms (in case of **2** or **3**, respectively), and introduced an additional double bond in the chain as well as the terminal amino-groups protected as *tert*-butyloxycarbonyl (Boc) or phthalimide (Phth) (in case of **2** or **3**, respectively). Deprotection of the Boc or Phth moieties with trifluoroacetic acid (TFA) and methylamine solution in ethanol (33 wt %), respectively, afforded $\mathbf{u}_2\mathbf{C}_{39}$-$\mathbf{NH}_2$, $\mathbf{u}_2\mathbf{C}_{44}$-$\mathbf{NH}_2$, $\mathbf{u}_3\mathbf{C}_{50}$-$\mathbf{NH}_2$, and $\mathbf{u}_3\mathbf{C}_{55}$-$\mathbf{NH}_2$ after chromatographic purification (see experimental details in the Supporting Information). The stereochemistry of the newly added double bonds was not controlled for the same reasons previously explained (*vide supra*). The theoretical number of possible isomers for each amine amounted to 2^n, with n = number of double bonds present in the chemical structure. Assuming no influence of these double bond configurations on the chemical reactivity of the terminal amino groups in $\mathbf{u}_m\mathbf{C}_n$-$\mathbf{NH}_2$, the theoretical number of possible isomers for unsaturated $\mathbf{C}_n$-**NDI**-$\mathbf{C}_n$ would then be $2(2^n)$.

The unsaturated NDIs were synthesized by condensation between the unsaturated amines and commercially available naphthalenedianhydride (**NDA**) *via* a modified microwave-assisted protocol (Scheme 2).[61−63] After chromatographic purification, the unsaturated NDIs were obtained in good yields (ranging from 75 to 85%) as not resolvable mixtures of stereoisomers (Scheme 2). Fully saturated $\mathbf{C}_{39}$-**NDI**-$\mathbf{C}_{39}$, $\mathbf{C}_{44}$-**NDI**-$\mathbf{C}_{44}$, and $\mathbf{C}_{50}$-**NDI**-$\mathbf{C}_{50}$ were synthesized by palladium on carbon (Pd/C, 10 wt % Pd content)-catalyzed hydrogenation of unsaturated $\mathbf{C}_n$-**NDI**-$\mathbf{C}_n$ at 110−115 °C (Scheme 2). Reaching high temperatures (reaction mixtures were heated up at reflux) was necessary to favor the solubilization of the partially hydrogenated reaction intermediates, significantly less soluble than the starting materials, and consequently allow exhaustive reduction of the double bonds. For this reason, a 2:1 toluene/ethyl valerate solvent mixture was used for the catalytic hydrogenation. Fully saturated $\mathbf{C}_{39}$-**NDI**-$\mathbf{C}_{39}$, $\mathbf{C}_{44}$-**NDI**-$\mathbf{C}_{44}$, and $\mathbf{C}_{50}$-**NDI**-$\mathbf{C}_{50}$ were finally obtained in high purity by means of Soxhlet extraction, applying different alkane solvents depending on the chain length of the desired saturated $\mathbf{C}_n$-**NDI**-$\mathbf{C}_n$ (see the experimental details in the Supporting Information). The saturated NDIs were insoluble in the used

https://dx.doi.org/10.1021/acsnano.0c06274
ACS Nano 2020, 14, 13865−13875

Scheme 1. Synthesis of u_2C_{39}-NH_2, u_2C_{44}-NH_2, u_3C_{50}-NH_2, and u_3C_{55}-NH_2

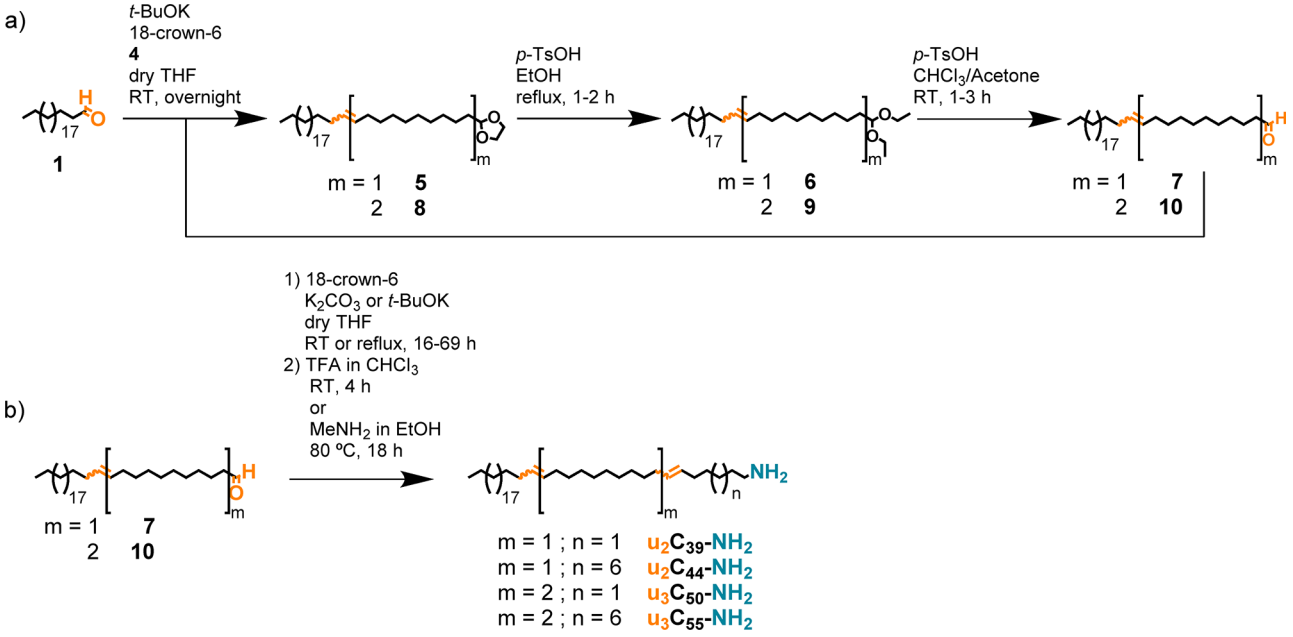

Scheme 2. Synthesis of Unsaturated u_2C_{39}-NDI-u_2C_{39}, u_2C_{44}-NDI-u_2C_{44}, u_3C_{50}-NDI-u_3C_{50}, and u_3C_{55}-NDI-u_3C_{55} and Saturated C_{39}-NDI-C_{39}, C_{44}-NDI-C_{44}, and C_{50}-NDI-C_{50}

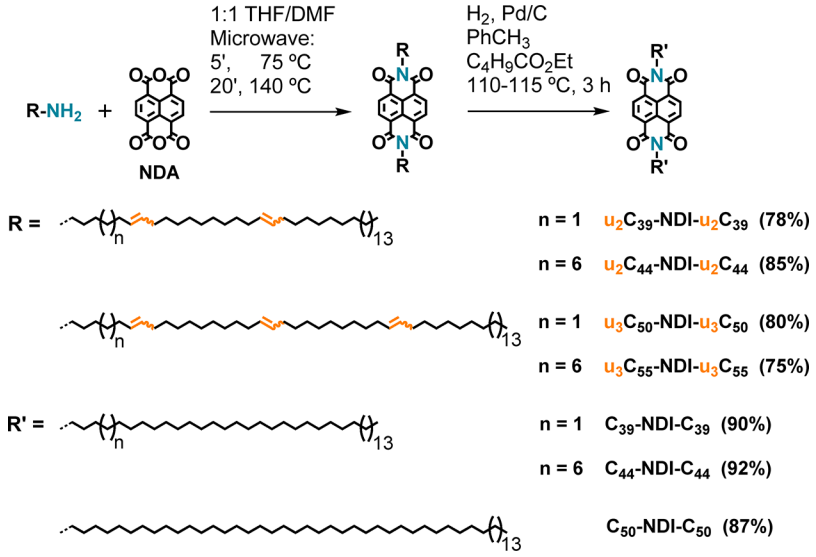

alkane solvents at room temperature, but they readily dissolved in the boiling solvents. This allowed for successful extraction at elevated temperatures and subsequent crystallization of the desired products upon cooling down of the extracted solutions.

All u_mC_n-NH_2 and unsaturated/saturated C_n-NDI-C_n were obtained as white waxes (u_mC_n-NH_2 and unsaturated C_n-NDI-C_n) and powders (saturated C_n-NDI-C_n). The full molecular characterization is reported in the Supporting Information, whereas we discuss here the thermal characterization carried out with differential scanning calorimetry (DSC) in view of the recent interest in thermal properties and crystallinity of discrete oligoethylene-based systems.[64,65] The DSC thermographs of u_3C_{50}-NH_2, u_3C_{50}-NDI-u_3C_{50}, and C_{50}-NDI-C_{50} are shown in Figure 1 as examples, whereas full DSC traces of all amines and **unsaturated/saturated** C_n-NDI-C_n can be found in the Supporting Information. All compounds reproducibly showed melting/crystallization transitions upon heating/cooling cycles (Figure 1 and the Supporting Information) without any sign of decomposition in the investigated temperature intervals. In general, the melting transitions of the amines occurred at lower temperatures compared to both unsaturated/saturated C_n-NDI-C_n featuring the same number of carbon atoms per chain. In the specific case of u_3C_{50}-NH_2, the presence of three double bonds, with various *E*/*Z* configurations in the molecular structures resulted in two broad thermal transitions (Figure 1, blue trace), which we associated with a collection of individual melting processes of the different geometrical isomers. Above 52 °C, solid u_3C_{50}-NH_2 reached the molten state (Figure 1, blue trace). The incorporation of u_3C_{50}-NH_2 into the skeleton of u_3C_{50}-NDI-u_3C_{50} resulted in a single and narrow melting transition at 55.5 °C (Figure 1, orange trace). We attributed the sharp feature of

https://dx.doi.org/10.1021/acsnano.0c06274
ACS Nano 2020, 14, 13865−13875

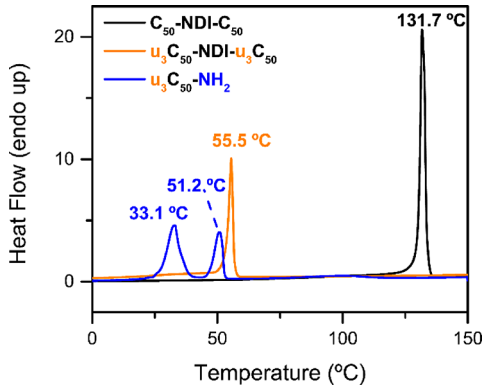

Figure 1. DSC thermograms (endo up; second heating ramp; 5 °C/min) of u_3C_{50}-NH_2 (blue trace), u_3C_{50}-NDI-u_3C_{50} (orange trace), and C_{50}-NDI-C_{50} (black trace).

such a melting transition to enhanced crystallinity of **u_3C_{50}-NDI-u_3C_{50}** deriving from the tendency of the NDI cores to arrange regularly in bulk materials.[61,66] Finally, exhaustive hydrogenation of the double bonds to give **C_{50}-NDI-C_{50}** pushed the melting transition to 131.7 °C (Figure 1, black trace), ~76 °C higher than **u_3C_{50}-NDI-u_3C_{50}**. We concluded that removal of the internal unsaturations introduced higher regularity in the alkyl chains and, hence, significantly promoted their ordered packing (crystallinity) in the solid state. The trend in melting points observed for unsaturated/saturated **C_n-NDI-C_n** nicely fits within the general difference in melting points of unsaturated/saturated fatty acids and esters.[67,68]

Self-Assembly of Saturated/Unsaturated C_n-NDI-C_n with $n \geq 39$ at the 1-PO/HOPG Interface. We first studied the self-assembly of saturated **C_{39}-NDI-C_{39}** and **C_{44}-NDI-C_{44}** at the 1-PO/HOPG interface. Solutions of these NDIs (0.4 mg/mL in 1-PO) were drop cast at 100 °C onto freshly cleaved HOPG substrates and subsequently imaged. The UV–vis spectrum of a **C_{44}-NDI-C_{44}** solution in 1-PO (0.4 mg/mL) which underwent a similar thermal treatment (heated at 100 °C and cooled down to room temperature) showed the typical well-resolved vibronic bands at 380, 360, and 342 nm of the NDI chromophore and a flat baseline (Figure S41). Especially this last aspect confirmed the homogeneity of the drop-cast solutions under the experimental conditions. A selection of STM images obtained with these saturated derivatives is reported in Figure 2a, b (for **C_{39}-NDI-C_{39}**) and Figure 2d, e (for **C_{44}-NDI-C_{44}**). The compounds self-assembled into lamellar structures, visualized as alternating dark and bright regions (Figure 2a–c). The bright protrusions account for the NDI cores, the conducting moieties of the chemical architectures, whereas the dark region corresponds to the saturated carbon chains. This is coherent with previous **C_n-NDI-C_n** designs with $n \geq 13$ that consistently afforded lamellar morphologies at the liquid/HOPG interface.[54,55] The NDI cores lay flat and next to each other on the surface in the lamellae, whereas the alkyl chains are either interdigitating[54] (lamellar phase A) or diagonally assembled[54] (lamellar phase B) (Figure 2a). For a pictorial representations of lamellar phase A and lamellar phase B see Figure 3. A close inspection to the self-assembled monolayers of **C_{39}-NDI-C_{39}** (Figure 2a) and **C_{44}-NDI-C_{44}** (Figure 2d) highlighted a decreased tendency to form the phase B, as well as a misalignment of the NDI cores in phase A, upon extending the alkyl chain length compared to the shorter **C_n-NDI-C_n** (n = 28, 33) previously investigated.[53] Both features induce disorder at the whole-surface level, as visualized by the enhanced formation of less straight and more curved lamellar arrangements with respect to the shorter **C_n-NDI-C_n** (n = 28, 33).[53] The large-

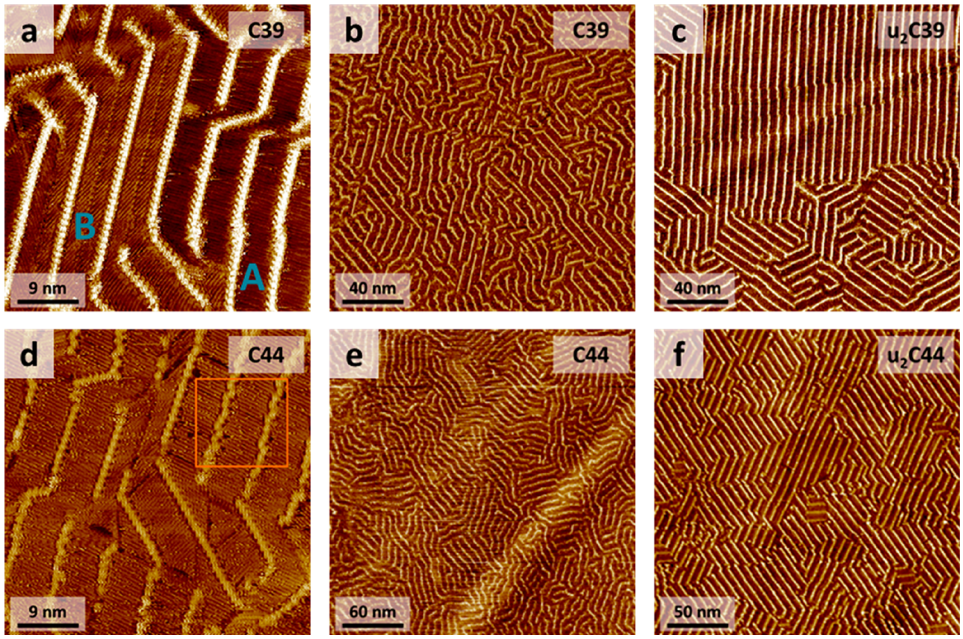

Figure 2. STM images of (a) two different assemblies of C_{39}-NDI-C_{39}: an interdigitated assembly (lamellar phase A, marked by the letter "A" in the STM image) and a non-interdigitated diagonal-assembly (lamellar phase B, marked by the letter "B" in the STM image) (45 nm × 45 nm, V_{tip} = 1 V, I_{set} = 100 pA); (b) C_{39}-NDI-C_{39} (large-area scan of 200 nm × 200 nm, V_{tip} = 1 V, I_{set} = 100 pA); (c) u_2C_{39}-NDI-u_2C_{39} (large-area scan of 200 nm × 200 nm, V_{tip} = 1 V, I_{set} = 60 pA); (d) C_{44}-NDI-C_{44} showing the predominant presence of lamellar phase A (45 nm × 45 nm, V_{tip} = 1.3 V, I_{set} = 100 pA). The orange box designates the tortuous NDI cores; (e) C_{44}-NDI-C_{44} (large-area scan of 300 nm × 300 nm, V_{tip} = 1 V, I_{set} = 100 pA); (f) u_2C_{44}-NDI-u_2C_{44} (large-area scan of 200 nm × 200 nm, V_{tip} = 1.3 V, I_{set} = 100 pA).

https://dx.doi.org/10.1021/acsnano.0c06274
ACS Nano 2020, 14, 13865–13875

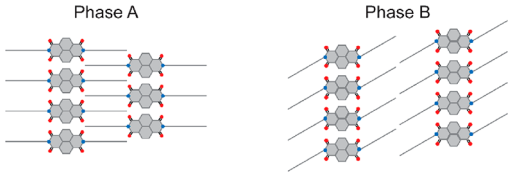

Figure 3. Cartoons depicting qualitative aspects of lamellar phase A (interdigitation of the carbon chains, flat NDI cores), and lamellar phase B (non-interdigitated and diagonal organization of the carbon chains, flat NDI cores). Nitrogen atoms are schematically represented in blue, oxygen atoms in red, and carbon atoms in gray.

area scans of C_{44}-NDI-C_{44} (Figure 2e) reveal the significant preference of these molecules to misalign and deviate from the "canonical" description of the lamellar morphologies (see the area delimited by the orange square in Figure 2d, for example). We anticipate that this is a consequence of extending the length of the carbon chains (*vide infra*).

Qualitatively more ordered self-assembled monolayers were obtained upon drop casting 1-PO solutions of u_2C_{39}-NDI-u_2C_{39} and u_2C_{44}-NDI-u_2C_{44} onto freshly cleaved HOPG (Figure 2c for u_2C_{39}-NDI-u_2C_{39}, and Figure 2f for u_2C_{44}-NDI-u_2C_{44}). The two unsaturated derivatives gave place to lamellae (phase A) with the typical alternation of dark (carbon chains) and bright (NDI) areas in the STM images (Figure 2c, f).[53−55] The contrast in order between the monolayers obtained from u_2C_{39}-NDI-u_2C_{39} and u_2C_{44}-NDI-u_2C_{44} and their saturated counterparts is evident (compare Figure 2b, c, and 2e, f). Whenever the internal double bonds were present in the molecular structure, the monolayers generated show significantly enhanced order. These results further suggested that internal double bonds placed in long-carbon-chain derivatives can be exploited as order-inducing functional groups on surfaces, although the ordered domains obtained with u_2C_{39}-NDI-u_2C_{39} and u_2C_{44}-NDI-u_2C_{44} did not reach the same extensions as those with shorter unsaturated uC_{28}-NDI-uC_{28} and uC_{33}-NDI-uC_{33}.[53] Moreover, the same qualitative trend of increasing disorder upon extending the number of carbon atoms in the chain length also occurred with u_2C_{39}-NDI-u_2C_{39} and u_2C_{44}-NDI-u_2C_{44}, in line with the previous discussion on C_{39}-NDI-C_{39} and C_{44}-NDI-C_{44}. Both unsaturated and saturated systems were strongly influenced by the packing of the long carbon chains. The unit-cell parameters for C_{39}-NDI-C_{39} and C_{44}-NDI-C_{44}, and u_2C_{39}-NDI-u_2C_{39} and u_2C_{44}-NDI-u_2C_{44} are all reported in Table 1.

Carbon-Chain Arrangements and Combinatorial Selection upon Self-Assembly. With unsaturated C_n-NDI-C_n with $n \leq 33$—only one internal double bond and either 28 or 33 carbon atoms per carbon chain—the *EE*-configured isomer showed preferential physisorption.[53] Additional bright protrusions symmetrically placed with respect to the NDI cores in the STM images allowed us to identify such internal double bonds. The longer chain u_2C_{44}-NDI-u_2C_{44} enabled the identification of additional bright protrusions due to the presence of two internal double bonds per carbon chain (Figure 4, selected double bonds are marked as orange or blue

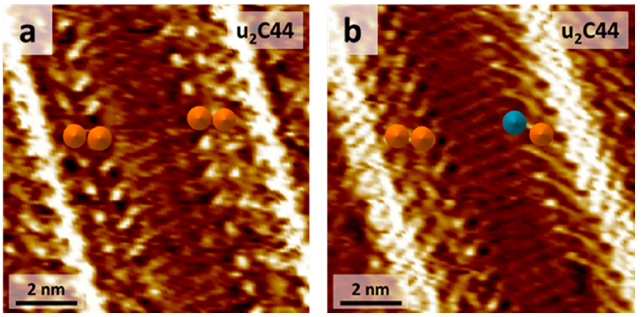

Figure 4. STM images of (a) u_2C_{44}-NDI-u_2C_{44} with all *E*-configured double bonds (bright protrusions next to the NDI core) (10 nm × 10 nm, V_{tip} = 1.3 V, I_{set} = 100 pA); (b) u_2C_{44}-NDI-u_2C_{44} with double bonds in *E*- and *Z*-configuration (10 nm × 10 nm, V_{tip} = 1.3 V, I_{set} = 200 pA). *E*-configured double bonds are marked by the orange dots, whereas *Z*-configured double bonds are highlighted by the blue dot.

dots). The STM images shown in Figure 4 highlighted the presence of two different isomers within the self-assembled monolayer of u_2C_{44}-NDI-u_2C_{44} in lamellar phase A. These isomers differed by the configuration of the double bond more remote to the NDI core, namely, the C═C between carbon atoms 22 and 23, while the double bond closer to the NDI core always appeared in the *E*-configuration (the *E*-configured unsaturation is marked as an orange dot in Figure 4). The distinction between *E*- and *Z*-configured double bonds in the STM images was based on the appearance of the aliphatic chains and was supported by previous literature on *E*-oleic acid and *Z*-oleylamine.[69] The carbon chains featuring *E*-double bonds assume zigzag conformations on HOPG in a very similar fashion to alkyl chains, whereas the *Z*-configured tails clearly show bending of the carbon chain forced by the stringent geometry of the *Z*-configuration that cannot be compensated due to forbidden rotation around the double bond.[69] In this respect, Figure 4a, b displays both behaviors, with Figure 4b showing pronounced bending of the carbon chains caused by the *Z*-configured unsaturation (blue dot in Figure 4b) more remote from the NDI core.

The consistency of the *E*-configuration for the double bonds closer to the NDI core seemed to suggest the combinatorial

Table 1. Determined Unit-Cell Parameters of the Self-Assembled Monolayers of Saturated and Unsaturated C_n-NDI-C_n at the 1-PO/HOPG Interface

compd	*a* (nm)	*b* (nm)	*γ* (deg)	phase	NDI core
C_{39}-NDI-C_{39}	6.16 ± 0.08	0.95 ± 0.04	88.76 ± 0.71	A + B	flat
u_2C_{39}-NDI-u_2C_{39}	6.07 ± 0.11	0.92 ± 0.02	87.37 ± 2.44	A	flat
C_{44}-NDI-C_{44}	6.91 ± 0.19	0.91 ± 0.09	87.10 ± 1.49	A + B	flat
u_2C_{44}-NDI-u_2C_{44}	6.63 ± 0.13	0.94 ± 0.03	86.58 ± 2.14	A	flat
C_{50}-NDI-C_{50}	7.66 ± 0.16	0.92 ± 0.02	85.63 ± 2.39	A	flat
u_3C_{50}-NDI-u_3C_{50}	12.08 ± 0.46	0.62 ± 0.13	86.36 ± 2.00	C	tilted
u_3C_{55}-NDI-u_3C_{55}	13.07 ± 0.20	0.52 ± 0.01	86.84 ± 3.31	C	tilted

https://dx.doi.org/10.1021/acsnano.0c06274
ACS Nano 2020, 14, 13865−13875

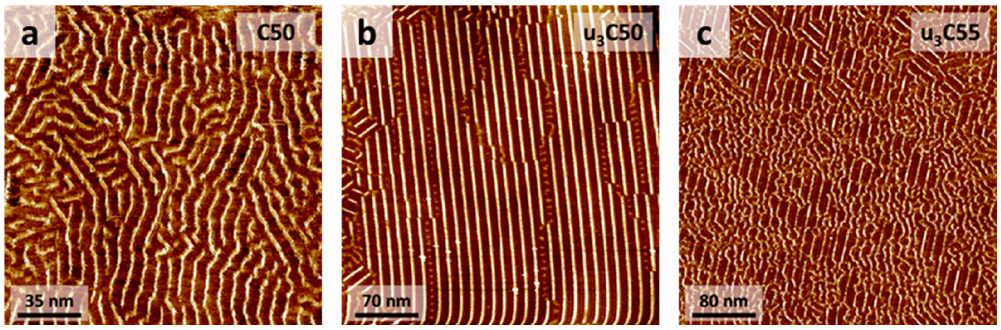

Figure 5. STM images of (a) C_{50}-NDI-C_{50} (175 nm × 175 nm, V_{tip} = 1 V, I_{set} = 100 pA); (b) u_3C_{50}-NDI-u_3C_{50} (350 nm × 350 nm, V_{tip} = 1 V, I_{set} = 100 pA); (c) u_3C_{55}-NDI-u_3C_{55} (400 nm × 400 nm, (V_{tip} = 1 V, (I_{set} = 100 pA) at the 1-PO/HOPG interface.

selection for *E*-configured geometrical isomers at these specific double bond position and carbon chain length (C_{44}). This was not expected, because the *Z*-configurations were the most abundant double bond geometries produced in the synthesis of u_mC_n-NH_2 due to Wittig olefination conditions applied (non-stabilized phosphorus ylide).[59] Although the selection rule for the first unsaturation appeared to be more stringent, more freedom was associated to the configuration of the more remote double bond, which led to the coexistence of *E*- or *Z*-configurations. Both *EE* and *ZE* isomers (the double-bond configurations are given per one carbon chain only) were recruited in the self-assembly process on HOPG as result of the adaptivity of these self-assembled monolayers. The interplay between dynamics and thermodynamics in self-assembled monolayers at the liquid−solid interface brought to the selection of the geometrical isomers forming the most stable pattern on the surface, whereas the other stereoisomers of u_2C_{44}-NDI-u_2C_{44} remained in the overlying liquid phase and were not imaged. Finally, in view of the rationalization of the observed assemblies and the general discussion of kinetics and thermodynamics, we stress the consistency of the imaged self-assembled monolayers of all saturated and unsaturated C_n-NDI-C_n after prolonged exposure (8 h) to the overlying C_n-NDI-C_n solutions or rinsing with fresh 1-PO to remove the excess of non-physisorbed C_n-NDI-C_n. Both aspects strongly suggest that all C_n-NDI-C_n systems had reached thermodynamic equilibrium at the 1-PO/HOPG interface.

Self-Assembly of Saturated/Unsaturated C_n-NDI-C_n with $n \geq 50$ at the 1-PO/HOPG Interface. Next, we investigated C_{50}-NDI-C_{50}, u_3C_{50}-NDI-u_3C_{50}, and u_3C_{55}-NDI-u_3C_{55} at the 1-PO/HOPG interface. The samples were prepared by drop casting at high temperatures (150 °C) to favor the complete solubilization of the compounds, especially in the case of C_{50}-NDI-C_{50}. Typical STM images of the self-assembled monolayers obtained with C_{50}-NDI-C_{50}, u_3C_{50}-NDI-u_3C_{50}, and u_3C_{55}-NDI-u_3C_{55} are shown in Figure 5. The misalignment previously discussed with C_{44}-NDI-C_{44} was also observed in the STM images of C_{50}-NDI-C_{50} (Figure 5a), confirming the trend to lose the "straight-line shape" upon extending the carbon chain length in saturated C_n-NDI-C_n. In stark contrast, u_3C_{50}-NDI-u_3C_{50} afforded sharp and straight arrangements of NDI cores on HOPG (Figure 5b). The comparison between C_{50}-NDI-C_{50} and u_3C_{50}-NDI-u_3C_{50} furnished additional confirmation of the powerful role played by internal unsaturations as order-inducing structural motifs[53] at the liquid/HOPG interface. However, this tendency was counterbalanced by the order-disrupting effect due to the increased length of the carbon chains, which was mostly evident with saturated C_n-NDI-C_n (for additional STM images, see the Supporting Information). Minor inconsistencies in the distance between bright arrays (regions of the NDI cores) might be detected in the STM images and could be assigned to the adsorption of only a part of the carbon chain, *i.e.*, with part of the tail on the surface and the rest upright in the overlying liquid phase. Particularly in the case of the unsaturated C_n-NDI-C_n, possible local deposition of uC_n-NDI-uC_n with differently configured internal double bonds could create local disorders, which might locally change the contrast. The discussion of both these aspects is general and valid also for the saturated and unsaturated C_n-NDI-C_n ($39 \geq n \geq 44$) previously presented. Hence, the internal double bonds impart order only locally with unsaturated C_n-NDI-C_n with $n \geq 39$, whereas they induced long-range order in the case of unsaturated C_n-NDI-C_n with $n \leq 33$.[53] The STM images of the self-assembled monolayers of u_3C_{55}-NDI-u_3C_{55} probably represented the most direct manifestation of the antagonistic interplay between the simultaneous presence of internal double bonds and longer chains (Figure 5c). The phase separation between NDI cores and carbon chains was still visible in the STM images, but the extent of order was drastically reduced and most of the surface was covered by randomly organized domains (Figure 5c).

A close inspection of the STM images of Figure 5b, c showed only limited areas characterized by a distinct organization (Figure 6). As previously discussed for u_2C_{44}-NDI-u_2C_{44}, also in this case the locally ordered regions on the monolayers were associated to the combinatorial selection of one stereoisomer for u_3C_{50}-NDI-u_3C_{50} and u_3C_{55}-NDI-u_3C_{55}.

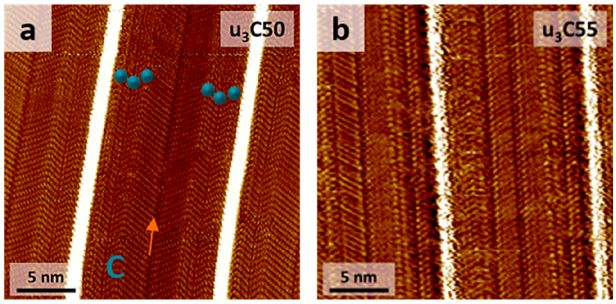

Figure 6. STM images of (a) u_3C_{50}-NDI-u_3C_{50} (25 nm × 25 nm, V_{tip} = 0.9 V, I_{set} = 40 pA), and (b) u_3C_{55}-NDI-u_3C_{55} (25 nm × 25 nm, V_{tip} = 1.3 V, I_{set} = 25 pA) at the 1-PO/HOPG interface showing the "phase C" lamellar assembly. The blue dots indicate the positions of the Z-configured double bonds and the orange arrow points out the junction between two lamellae.

https://dx.doi.org/10.1021/acsnano.0c06274
ACS Nano 2020, 14, 13865−13875

In these specific examples, HOPG locally selected fully *Z*-configured double bonds, as suggested by the particularly evident bending of the chain caused by the *Z*-configuration of the carbon chains of $\mathbf{u_3C_{50}}$-**NDI**-$\mathbf{u_3C_{50}}$ (Figure 6a; for an enlarged image see Figure S44). The selection of one geometrical isomer only in a highly complex mixture of stereoisomers is a peculiar property of the system and confirms the high adaptivity of the $\mathbf{C}_n$-**NDI**-$\mathbf{C}_n$ monolayers at the 1-PO/HOPG interface. Besides these conclusions, the introduction of the third unsaturation in $\mathbf{u_3C_{50}}$-**NDI**-$\mathbf{u_3C_{50}}$ and $\mathbf{u_3C_{55}}$-**NDI**-$\mathbf{u_3C_{55}}$ also brought to the discovery of a lamellar packing mode for the $\mathbf{C}_n$-**NDI**-$\mathbf{C}_n$ that we denoted as "lamellar phase C". In this organization, the carbon chains are assembled in a parallel lamellar fashion and create a junction between the tails belonging to two parallel arrays of NDIs (Figure 6a; Figures S44 and S45). These features differ strongly from those of the interdigitating (phase A) or diagonal (phase B) lamellar modes of Figure 3.[54,55] A schematic representation of the lamellar phase C created by the $\mathbf{C}_n$-**NDI**-$\mathbf{C}_n$ with $n \geq 50$ is shown in Figure 7.

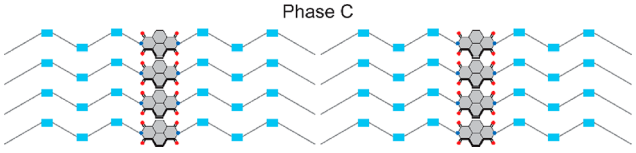

Figure 7. Cartoon depicting qualitative aspects of lamellar phase C (non-interdigitated organization of the unsaturated carbon chains, tilted NDI cores). Nitrogen atoms are schematically represented in blue, oxygen atoms in red, carbon atoms in gray, and the *Z*-configured internal double bonds are shown as light blue rectangles.

Further confirmation of the difference among the lamellar "phase C" and phase A and phase B packing modes was obtained from the determination of the local unit cell (Table 1). The formation of a lamellar morphology was justified by a practically rectangular unit cell, as supported by the ~86° value for the γ-angle for both $\mathbf{u_3C_{50}}$-**NDI**-$\mathbf{u_3C_{50}}$ and $\mathbf{u_3C_{55}}$-**NDI**-$\mathbf{u_3C_{55}}$ (Table 1). Moreover, the absence of interdigitation or diagonal deposition of the carbon chains resulted in increasing the lateral distance between parallel lamellae, which is measured by the *a* value. Indeed, the increase in *a* value by ~6−7 nm upon going from $\mathbf{u_2C_{44}}$-**NDI**-$\mathbf{u_2C_{44}}$ to $\mathbf{u_3C_{50}}$-**NDI**-$\mathbf{u_3C_{50}}$ (extension of 6 carbon atoms per chain) and $\mathbf{u_3C_{55}}$-**NDI**-$\mathbf{u_3C_{55}}$ (extension of 11 carbon atoms per chain) can only be justified by a different arrangement of the carbon chains (Table 1). The most intriguing unit-cell parameter of the new phase C lamellar mode is the *b* value, namely, the distance between adjacent NDI cores within the same lamella. We obtained a *b* value of 0.62 ± 0.13 nm for $\mathbf{u_3C_{50}}$-**NDI**-$\mathbf{u_3C_{50}}$, and 0.52 ± 0.01 nm for $\mathbf{u_3C_{55}}$-**NDI**-$\mathbf{u_3C_{55}}$ (Table 1). Because the width of an NDI core is approximately 0.9 nm (width of the central naphthyl ring in the NDI core), an approximate *b* value for a closely packed system in which the NDI cores lay flat on the surface should amount to 0.9 nm. Congruously, *b* values determined for $\mathbf{u_2C_{39}}$-**NDI**-$\mathbf{u_2C_{39}}$ and $\mathbf{u_2C_{44}}$-**NDI**-$\mathbf{u_2C_{44}}$ (Table 1) and other systems[53,55] match with 0.9 ± 0.1 nm. The significantly smaller *b* value measured for $\mathbf{u_3C_{50}}$-**NDI**-$\mathbf{u_3C_{50}}$ and $\mathbf{u_3C_{55}}$-**NDI**-$\mathbf{u_3C_{55}}$ hints at a non-completely flat (tilted) deposition of the NDI cores. Considering the high tendency of NDIs to interact strongly with HOPG, we hypothesize that the non-flat deposition of the NDI cores is compensated by *intra*-lamellar and distorted π-interactions between adjacent NDIs, and enhanced van der Waals interactions between adjacent and more tightly-packed carbon chains. This is particularly interesting because it could offer prospects to merge the supramolecular chemistry typically occurring in solution, such as chemical recognition and supramolecular polymerizations, to surface-based supramolecular chemistry.

CONCLUSIONS

In summary, we reported the synthesis and self-assembly at the 1-PO/HOPG interface of new naphthalenediimides (NDIs) symmetrically functionalized with carbon chains comprising from 39 to 55 carbon atoms per chain ($\mathbf{C}_n$-**NDI**-$\mathbf{C}_n$, with $39 \leq n \leq 55$). The investigated NDIs differ by the presence/absence of two or three internal double bonds in the carbon chains (unsaturated and saturated $\mathbf{C}_n$-**NDI**-$\mathbf{C}_n$, respectively). In this work, we pushed the limits in terms of molecular design and order/disorder at the 1-PO/HOPG interface. We compared the outcome of the self-assembly of unsaturated and saturated $\mathbf{C}_n$-**NDI**-$\mathbf{C}_n$ with an identical number of carbon atoms per chain. The comparative study confirmed that the introduction of internal unsaturations along the carbon chains is pivotal to obtain ordered domains on HOPG. The dynamics and thermodynamics of these on-surface supramolecular systems allow for selecting the geometrical isomer(s) giving the most stable monolayer. However, the order-inducing effect of the internal double bonds is only local, because extending the length of the carbon chains causes misalignments in the packing of the carbon chains and induces disorder. Thus, the tiny energetic differences at this particular carbon-chain-length regime result in an antagonistic interplay between the presence of the internal double bonds and extended carbon chain lengths. Such interplay finds a compromise in the local formation of a new lamellar phase for $\mathbf{C}_n$-**NDI**-$\mathbf{C}_n$ with $n \geq 50$ ($\mathbf{u_3C_{50}}$-**NDI**-$\mathbf{u_3C_{50}}$ and $\mathbf{u_3C_{55}}$-**NDI**-$\mathbf{u_3C_{55}}$), denoted as phase C. In phase C, the carbon chains assemble in a parallel lamellar fashion and create a junction between the tails of parallel arrays of NDIs, whereas the aromatic cores do not lay flat on HOPG but assume a slightly tilted conformation. These aromatic cores should be available for establishing supramolecular contacts with either other NDIs within the same lamellar arrangement or other species in the solution phase. We highlight this latter aspect as a potential opportunity to combine supramolecular chemistry processes typically occurring in solution with self-assembled monolayers at the solid−liquid interface.

METHODS

Unless stated otherwise, all reagents and chemicals were obtained from commercial sources (TCI Chemicals and Sigma-Aldrich) at the highest purity available and used without further purification.

Microwave reactions were performed on a Biotage Initiator reactor.

Column chromatography was performed using a Grace Reveleris X2 equipped with an evaporative light scattering detector.

^{1}H NMR and ^{13}C NMR spectra were recorded either on a Varian Mercury Vx 400 MHz (100 MHz for ^{13}C), Varian Oxford AS 500 MHz (125 MHz for ^{13}C) or Bruker 600 MHz (150 MHz for ^{13}C) NMR spectrometers. Chemical shifts are given in ppm (δ) values relative to residual solvent or tetramethylsilane (TMS). Splitting patterns are labeled as s, singlet; d, doublet; t, triplet; q, quartet; p, pentet; m, multiplet.

Matrix-assisted laser desorption/ionization mass spectra were obtained on a PerSeptive Biosystems Voyager DE-PRO spectrometer

https://dx.doi.org/10.1021/acsnano.0c06274
ACS Nano 2020, 14, 13865−13875

or a Bruker autoflex speed spectrometer using α-cyano-4-hydroxycinnamic acid (CHCA) and 2-[(2E)-3-(4-tert-butylphenyl)-2-methylprop-2-enylidene]malononitrile (DCTB) as matrices.

Infrared spectra were recorded on a PerkinElmer Spectrum One 1600 FT-IR spectrometer or a PerkinElmer Spectrum Two FT-IR spectrometer, equipped with a PerkinElmer Universal ATR Sampler Accessory.

UV−vis absorption spectra were recorded on a Hewlett-Packard 8453 spectrometer, using 1 cm optical path quartz cuvettes.

Differential scanning calorimetry (DSC) measurements were carried out with a PerkinElmer Pyris 1 DSC under a nitrogen atmosphere with heating and cooling rates of 5 °C/min.

STM Measurements. All experiments were performed at room temperature (21−25 °C) under ambient conditions using an STM (Molecular Imaging) operating in constant-current mode at the 1-phenyloctane/HOPG interface. STM tips were prepared by mechanical cutting of Pt/Ir wire (90/10, diameter 0.25 mm, Goodfellow). Solutions were prepared by dissolving 0.4 mg/mL of C_n-NDI-C_n in 1-phenyloctane (>98.0%, purchased by TCI). The solutions were heated to 100 °C and subsequently drop cast onto a freshly cleaved HOPG surface (ZYB grade, Bruker AFM probes). The solutions of C_{50}-NDI-C_{50}, u_3C_{50}-NDI-u_3C_{50}, and u_3C_{55}-NDI-u_3C_{55} were heated to 150 °C prior to the deposition on HOPG due to solubility issues. During scanning the STM tip was immerged into the solution. All STM images were analyzed and processed using *WSxM 5.0*.[70] and *Gwyddion*.[71] The images in the main text were processed using the plane, flatten, and equalize functions in *WSxM*. In addition to that, for some of the images in the Supporting Information, the smooth function was used. All bias values are given with respect to a grounded tip.

ASSOCIATED CONTENT

Supporting Information

The Supporting Information is available free of charge at https://pubs.acs.org/doi/10.1021/acsnano.0c06274.

Synthetic procedures and characterization including ^{1}H NMR, ^{13}C NMR, and FT-IR spectra of all new synthesized compounds; DSC traces of all new synthesized compounds; UV−vis spectrum of C_{44}-NDI-C_{44} in 1-PO (0.4 mg/mL); additional STM images (PDF)

AUTHOR INFORMATION

Corresponding Authors

E. W. Meijer − *Institute for Complex Molecular Systems and Laboratory of Macromolecular and Organic Chemistry, Eindhoven University of Technology, Eindhoven 5600 MB, The Netherlands;* orcid.org/0000-0003-4126-7492; Email: e.w.meijer@tue.nl

Ben L. Feringa − *Stratingh Institute for Chemistry, University of Groningen, Groningen 9747 AG, The Netherlands;* orcid.org/0000-0003-0588-8435; Email: b.l.feringa@rug.nl

Authors

José Augusto Berrocal − *Stratingh Institute for Chemistry, University of Groningen, Groningen 9747 AG, The Netherlands; Institute for Complex Molecular Systems and Laboratory of Macromolecular and Organic Chemistry, Eindhoven University of Technology, Eindhoven 5600 MB, The Netherlands;* orcid.org/0000-0003-3435-8310

G. Henrieke Heideman − *Stratingh Institute for Chemistry, University of Groningen, Groningen 9747 AG, The Netherlands*

Bas F. M. de Waal − *Institute for Complex Molecular Systems and Laboratory of Macromolecular and Organic Chemistry, Eindhoven University of Technology, Eindhoven 5600 MB, The Netherlands*

Complete contact information is available at: https://pubs.acs.org/10.1021/acsnano.0c06274

Author Contributions

†J.A.B. and G.H.H. contributed equally to this work

Notes

The authors declare no competing financial interest.

ACKNOWLEDGMENTS

This work was supported financially by the European Research Council (ERC, advanced grant 694345 to B.L.F.), and the Ministry of Education, Culture and Science (Gravitation Program 024.001.035). Mr. Ralf Bovee (TU Eindhoven) is acknowledged for MALDI-TOF measurements. The authors thank Pieter van der Meulen (University of Groningen) for assistance during some NMR experiments.

REFERENCES

(1) Goronzy, D. P.; Ebrahimi, M.; Rosei, F.; Arramel; Fang, Y.; De Feyter, S.; Tait, S. L.; Wang, C.; Beton, P. H.; Wee, A. T. S.; Weiss, P. S.; Perepichka, D. F. Supramolecular Assemblies on Surfaces: Nanopatterning, Functionality, and Reactivity. *ACS Nano* **2018**, *12*, 7445−7481.

(2) Woodruff, P. *Modern Techniques of Surface Science*, 3rd ed.; Cambridge University Press: Cambridge, 2016.

(3) Van Hove, M. A. From Surface Science to Nanotechnology. Catal. *Catal. Today* **2006**, *113*, 133−140.

(4) *Surface Design: Applications in Bioscience and Nanotechnology*; Förch, R., Schönherr, H., Jenkins, A. T. A., Eds.; Wiley−VCH: Weinheim, Germany, 2009.

(5) Mali, K. S.; Pearce, N.; De Feyter, S.; Champness, N. R. Frontiers of Supramolecular Chemistry at Solid Surfaces. *Chem. Soc. Rev.* **2017**, *46*, 2520−2542.

(6) Slater (née Phillips), A. G.; Beton, P. H.; Champness, N. R. Two-Dimensional Supramolecular Chemistry on Surfaces. *Chem. Sci.* **2011**, *2*, 1440−1448.

(7) Casalini, S.; Bortolotti, C. A.; Leonardi, F.; Biscarini, F. Self-Assembled Monolayers in Organic Electronics. *Chem. Soc. Rev.* **2017**, *46*, 40−71.

(8) Katz, H. E.; Huang, J. Thin-Film Organic Electronic Devices. *Annu. Rev. Mater. Res.* **2009**, *39*, 71−92.

(9) Pathem, B. K.; Claridge, S. A.; Zheng, Y. B.; Weiss, P. S. Molecular Switches and Motors on Surfaces. *Annu. Rev. Phys. Chem.* **2013**, *64*, 605−630.

(10) Velpula, G.; Takeda, T.; Adisoejoso, J.; Inukai, K.; Tahara, K.; Mali, K. S.; Tobe, Y.; De Feyter, S. On the Formation of Concentric 2D Multicomponent Assemblies at the Solution−Solid Interface. *Chem. Commun.* **2017**, *53*, 1108−1111.

(11) Xue, Y.; Zimmt, M. B. Patterned Monolayer Self-Assembly Programmed by Side Chain Shape: Four-Component Gratings. *J. Am. Chem. Soc.* **2012**, *134*, 4513−4516.

(12) Hipps, K. W.; Scudiero, L.; Barlow, D. E.; Cooke, M. P. A Self-Organized 2-Dimensional Bifunctional Structure Formed by Supramolecular Design. *J. Am. Chem. Soc.* **2002**, *124*, 2126−2127.

(13) Verstraete, L.; Greenwood, J.; Hirsch, B. E.; De Feyter, S. Self-Assembly under Confinement: Nanocorrals for Understanding Fundamentals of 2D Crystallization. *ACS Nano* **2016**, *10*, 10706−10715.

(14) Verstraete, L.; Smart, J.; Hirsch, B. E.; De Feyter, S. Unidirectional Supramolecular Self-Assembly inside Nanocorrals *via In Situ* STM Nanoshaving. *Phys. Chem. Chem. Phys.* **2018**, *20*, 27482−27489.

(15) Verstraete, L.; Szabelski, P.; Braganca, A. M.; Hirsch, B. E.; De Feyter, S. Adaptive Self-Assembly in 2D Nanoconfined Spaces:

Dealing with Geometric Frustration. *Chem. Mater.* **2019**, *31*, 6779−6786.
(16) Klappenberger, F.; Zhang, Y.-Q.; Björk, J.; Klyatskaya, S.; Ruben, M.; Barth, J. V. On-Surface Synthesis of Carbon-Based Scaffolds and Nanomaterials Using Terminal Alkynes. *Acc. Chem. Res.* **2015**, *48*, 2140−2150.
(17) Cirera, B.; Giménez-Agulló, N.; Björk, J.; Martínez-Peña, F.; Martin-Jimenez, A.; Rodriguez-Fernandez, J.; Pizarro, A. M.; Otero, R.; Gallego, J. M.; Ballester, P.; Galan-Mascaros, J. R.; Ecija, D. Thermal Selectivity of Intermolecular *versus* Intramolecular Reactions on Surfaces. *Nat. Commun.* **2016**, *7*, 11002−11009.
(18) Zuzak, R.; Pozo, I.; Engelund, M.; Garcia-Lekue, A.; Vilas-Varela, M.; Alonso, J. M.; Szymonski, M.; Guitián, E.; Pérez, D.; Godlewski, S.; Peña, D. Synthesis and Reactivity of a Trigonal Porous Nanographene on a Gold Surface. *Chem. Sci.* **2019**, *10*, 10143−10148.
(19) Grill, L.; Hecht, S. Covalent On-Surface Polymerization. *Nat. Chem.* **2020**, *12*, 115−130.
(20) Blake, M. M.; Nanayakkara, S. U.; Claridge, S. A.; Fernandez-Torres, L. C.; Sykes, E. C. H.; Weiss, P. S. Identifying Reactive Intermediates in the Ullmann Coupling Reaction by Scanning Tunneling Microscopy and Spectroscopy. *J. Phys. Chem. A* **2009**, *113*, 13167−13172.
(21) Lafferentz, L.; Eberhardt, V.; Dri, C.; Africh, C.; Comelli, G.; Esch, F.; Hecht, S.; Grill, L. Controlling On-Surface Polymerization by Hierarchical and Substrate-Directed Growth. *Nat. Chem.* **2012**, *4*, 215−220.
(22) Cardenas, L.; Gutzler, R.; Lipton-Duffin, J.; Fu, C.; Brusso, J. L.; Dinca, L. E.; Vondráček, M.; Fagot-Revurat, Y.; Malterre, D.; Rosei, F.; Perepichka, D. F. Synthesis and Electronic Structure of a Two Dimensional P-Conjugated Polythiophene. *Chem. Sci.* **2013**, *4*, 3263−3268.
(23) Bieri, M.; Nguyen, M.-T.; Gröning, O.; Cai, J.; Treier, M.; Aït-Mansour, K.; Ruffieux, P.; Pignedoli, C. A.; Passerone, D.; Kastler, M.; Müllen, K.; Fasel, R. Two-Dimensional Polymer Formation on Surfaces: Insight into the Roles of Precursor Mobility and Reactivity. *J. Am. Chem. Soc.* **2010**, *132*, 16669−166769.
(24) Elemans, J. A. A. W.; Lei, S.; De Feyter, S. Molecular and Supramolecular Networks on Surfaces: From Two-Dimensional Crystal Engineering to Reactivity. *Angew. Chem., Int. Ed.* **2009**, *48*, 7298−7332.
(25) Krüger, J.; García, F.; Eisenhut, F.; Skidin, D.; Alonso, J. M.; Guitián, E.; Pérez, D.; Cuniberti, G.; Moresco, F.; Peña, D. Decacene: On-Surface Generation. *Angew. Chem.* **2017**, *129*, 12107−12110.
(26) Pozo, I.; Guitián, E.; Pérez, D.; Peña, D. Synthesis of Nanographenes, Starphenes, and Sterically Congested Polyarenes by Aryne Cyclotrimerization. *Acc. Chem. Res.* **2019**, *52*, 2472−2481.
(27) Pavliček, N.; Schuler, B.; Collazos, S.; Moll, N.; Pérez, D.; Guitián, E.; Meyer, G.; Peña, D.; Gross, L. On-Surface Generation and Imaging of Arynes by Atomic Force Microscopy. *Nat. Chem.* **2015**, *7*, 623−628.
(28) Ilan, B.; Florio, G. M.; Hybertsen, M. S.; Berne, B. J.; Flynn, G. W. Scanning Tunneling Microscopy Images of Alkane Derivatives on Graphite: Role of Electronic Effects. *Nano Lett.* **2008**, *8*, 3160−3165.
(29) Mali, K. S.; Adisoejoso, J.; Ghijsens, E.; De Cat, I.; De Feyter, S. Exploring the Complexity of Supramolecular Interactions for Patterning at the Liquid-Solid Interface. *Acc. Chem. Res.* **2012**, *45*, 1309−1320.
(30) Barth, J. V.; Weckesser, J.; Cai, C.; Günter, P.; Bürgi, L.; Jeandupeux, O.; Kern, K. Building Supramolecular Nanostructures at Surfaces by Hydrogen Bonding. *Angew. Chem., Int. Ed.* **2000**, *39*, 1230−1234.
(31) Slater, A. G.; Perdigão, L. M. A.; Beton, P. H.; Champness, N. R. Surface-Based Supramolecular Chemistry Using Hydrogen Bonds. *Acc. Chem. Res.* **2014**, *47*, 3417−3427.
(32) Zhou, H.; Dang, H.; Yi, J.-H.; Nanci, A.; Rochefort, A.; Wuest, J. D. Frustrated 2D Molecular Crystallization. *J. Am. Chem. Soc.* **2007**, *129*, 13774−13775.
(33) Griessl, S.; Lackinger, M.; Edelwirth, M.; Hietschold, M.; Heckl, W. M. Self-Assembled Two-Dimensional Molecular Host-Guest Architectures From Trimesic Acid. *Single Mol.* **2002**, *3*, 25−31.
(34) Van Esch, J.; De Feyter, S.; Kellogg, R. M.; De Schryver, F.; Feringa, B. L. Self-Assembly of Bisurea Compounds in Organic Solvents and on Solid Substrates. *Chem. - Eur. J.* **1997**, *3*, 1238−1243.
(35) De Feyter, S.; Grim, P. C. M.; Van Esch, J.; Kellogg, R. M.; Feringa, B. L.; De Schryver, F. C. Nontrivial Differentiation between Two Identical Functionalities within the Same Molecule Studied by STM. *J. Phys. Chem. B* **1998**, *102*, 8981−8987.
(36) Gesquiere, A.; Abdel-Mottaleb, M. M. S.; De Feyter, S.; De Schryver, F. C.; Schoonbeek, F.; van Esch, J.; Kellogg, R. M.; Feringa, B. L.; Calderone, A.; Lazzaroni, R.; Bredas, J. L. Molecular Organization of Bis-Urea Substituted Thiophene Derivatives at the Liquid/Solid Interface Studied by Scanning Tunneling Microscopy. *Langmuir* **2000**, *16*, 10385−10391.
(37) Vijayaraghavan, S.; Ecija, D.; Auwärter, W.; Joshi, S.; Seufert, K.; Drach, M.; Nieckarz, D.; Szabelski, P.; Aurisicchio, C.; Bonifazi, D.; Barth, J. V. Supramolecular Assembly of Interfacial Nanoporous Networks with Simultaneous Expression of Metal-Organic and Organic-Bonding Motifs. *Chem. - Eur. J.* **2013**, *19*, 14143−14150.
(38) De Ruiter, G.; Lahav, M.; van der Boom, M. E. Pyridine Coordination Chemistry for Molecular Assemblies on Surfaces. *Acc. Chem. Res.* **2014**, *47*, 3407−3416.
(39) Stepanow, S.; Lingenfelder, M.; Dmitriev, A.; Spillmann, H.; Delvigne, E.; Lin, N.; Deng, X.; Cai, C.; Barth, J. V.; Kern, K. Steering Molecular Organization and Host−Guest Interactions Using Two-Dimensional Nanoporous Coordination Systems. *Nat. Mater.* **2004**, *3*, 229−233.
(40) Gutzler, R.; Fu, C.; Dadvand, A.; Hua, Y.; MacLeod, J. M.; Rosei, F.; Perepichka, D. F. Halogen Bonds in 2D Supramolecular Self-Assembly of Organic Semiconductors. *Nanoscale* **2012**, *4*, 5965.
(41) Yoon, J. K.; Son, W.; Chung, K.-H.; Kim, H.; Han, S.; Kahng, S.-J. Visualizing Halogen Bonds in Planar Supramolecular Systems. *J. Phys. Chem. C* **2011**, *115*, 2297−2301.
(42) Dickerson, P. N.; Hibberd, A. M.; Oncel, N.; Bernasek, S. L. Hydrogen-Bonding *versus* van Der Waals Interactions in Self-Assembled Monolayers of Substituted Isophthalic Acids. *Langmuir* **2010**, *26*, 18155−18161.
(43) Schneider, H.-J.; Yatsimirsky, A. K. *Principles and Methods in Supramolecular Chemistry*; John Wiley & Sons: Chichester, 2000.
(44) Atwood, J. L.; Barbour, L. J.; Heaven, M. W.; Raston, C. L. Controlling van Der Waals Contacts in Complexes of Fullerene C_{60}. *Angew. Chem., Int. Ed.* **2003**, *42*, 3254−3257.
(45) Schneider, H. J.; Schiestel, T.; Zimmermann, P. The Incremental Approach to Noncovalent Interactions: Coulomb and van Der Waals Effects in Organic Ion Pairs. *J. Am. Chem. Soc.* **1992**, *114*, 7698−7703.
(46) McNellis, E. R.; Meyer, J.; Reuter, K. Azobenzene at Coinage Metal Surfaces: Role of Dispersive van Der Waals Interactions. *Phys. Rev. B: Condens. Matter Mater. Phys.* **2009**, *80*, 205414.
(47) Sauer, J.; Ugliengo, P.; Garrone, E.; Saunders, V. R. Theoretical Study of van Der Waals Complexes at Surface Sites in Comparison with the Experiment. *Chem. Rev.* **1994**, *94*, 2095−2160.
(48) Zaremba, E.; Kohn, W. Van der Waals Interaction between an Atom and a Solid Surface. *Phys. Rev. B* **1976**, *13*, 2270−2285.
(49) Galanti, A.; Diez-Cabanes, V.; Santoro, J.; Valášek, M.; Minoia, A.; Mayor, M.; Cornil, J.; Samorì, P. Electronic Decoupling in C_3-Symmetrical Light-Responsive Tris(Azobenzene) Scaffolds: Self-Assembly and Multiphotochromism. *J. Am. Chem. Soc.* **2018**, *140*, 16062−16070.
(50) Hou, I. C.-Y.; Diez-Cabanes, V.; Galanti, A.; Valasek, M.; Mayor, M.; Cornil, J.; Narita, A.; Samori, P.; Mullen, K. Photomodulation of Two-Dimensional Self-Assembly of Azobenzene−Hexa-Peri-Hexabenzocoronene−Azobenzene Triads. *Chem. Mater.* **2019**, *31*, 6979−6985.
(51) Ciesielski, A.; El Garah, M.; Haar, S.; Kovaricek, P.; Lehn, J.-M.; Samori, P. Dynamic Covalent Chemistry of Bisimines at the

https://dx.doi.org/10.1021/acsnano.0c06274
ACS Nano 2020, 14, 13865−13875

Solid/Liquid Interface Monitored by Scanning Tunnelling Microscopy. *Nat. Chem.* **2014**, *6*, 1017−1023.
(52) Corbett, P. T.; Leclaire, J.; Vial, L.; West, K. R.; Wietor, J.-L.; Sanders, J. K. M.; Otto, S. Dynamic Combinatorial Chemistry. *Chem. Rev.* **2006**, *106*, 3652−3711.
(53) Berrocal, J. A.; Heideman, G. H.; de Waal, B. F. M.; Enache, M.; Havenith, R. W. A.; Stohr, M.; Meijer, E. W.; Feringa, B. L. Engineering Long-Range Order in Supramolecular Assemblies on Surfaces: The Paramount Role of Internal Double Bonds in Discrete Long-Chain Naphthalenediimides. *J. Am. Chem. Soc.* **2020**, *142*, 4070−4078.
(54) Kleiner-Shuhler, L.; Brittain, R.; Johnston, M. R.; Hipps, K. W. Scanning Tunneling Microscopy and Orbital-Mediated Tunneling Spectroscopy of N, N ′-Dioctyl-1,8:4,5-Naphthalenediimide Adsorbed on Highly Ordered Pyrolytic Graphite from Various Solvents and in Different Environments. *J. Phys. Chem. C* **2008**, *112*, 14907−14912.
(55) Miyake, Y.; Nagata, T.; Tanaka, H.; Yamazaki, M.; Ohta, M.; Kokawa, R.; Ogawa, T. Entropy-Controlled 2D Supramolecular Structures of N, N ′-Bis(n -Alkyl)Naphthalenediimides on a HOPG Surface. *ACS Nano* **2012**, *6*, 3876−3887.
(56) Berrocal, J. A.; Teyssandier, J.; Goor, O. J. G. M.; De Feyter, S.; Meijer, E. W. Supramolecular Loop Stitches of Discrete Block Molecules on Graphite: Tunable Hydrophobicity by Naphthalenediimide End-Capped Oligodimethylsiloxane. *Chem. Mater.* **2018**, *30*, 3372−3378.
(57) Igner, E.; Paynter, O.; Simmonds, D. J.; Whiting, M. C. Studies on the Synthesis of Linear Aliphatic Compounds. Part 2. The Realisation of a Strategy for Repeated Molecular Doubling. *J. Chem. Soc., Perkin Trans. 1* **1987**, 2447−2454.
(58) Bidd, I.; Whiting, M. C. The Synthesis of Pure N-Paraffins with Chain-Lengths between One and Four Hundred. *J. Chem. Soc., Chem. Commun.* **1985**, 543−544.
(59) Carey, F. A.; Sundberg, R. J. *Advanced Organic Chemistry—Part B: Reactions and Synthesis*, fifth ed.; Springer-Verlag: New York, 2007.
(60) van Genabeek, B.; De Waal, B. F. M.; Palmans, A. R. A.; Meijer, E. W. Discrete Oligodimethylsiloxane−Oligomethylene Di- and Triblock Co-Oligomers: Synthesis, Self-Assembly and Molecular Organisation. *Polym. Chem.* **2018**, *9*, 2746−2758.
(61) Berrocal, J. A.; Zha, R. H.; De Waal, B. F. M.; Lugger, J. A. M.; Lutz, M.; Meijer, E. W. Unraveling the Driving Forces in the Self-Assembly of Monodisperse Naphthalenediimide-Oligodimethylsiloxane Block Molecules. *ACS Nano* **2017**, *11*, 3733−3741.
(62) Salerno, F.; Berrocal, J. A.; Haedler, A. T.; Zinna, F.; Meijer, E. W.; Di Bari, L. Highly Circularly Polarized Broad-Band Emission from Chiral Naphthalene Diimide-Based Supramolecular Aggregates. *J. Mater. Chem. C* **2017**, *5*, 3609−3615.
(63) Bartocci, S.; Berrocal, J. A.; Guarracino, P.; Grillaud, M.; Franco, L.; Mba, M. Peptide-Driven Charge-Transfer Organogels Built from Synergetic Hydrogen Bonding and Pyrene-Naphthalenediimide Donor-Acceptor Interactions. *Chem. - Eur. J.* **2018**, *24*, 2920−2928.
(64) Lacombe, J.; Pearson, S.; Pirolt, F.; Norsic, S.; D'Agosto, F.; Boisson, C.; Soulié-Ziakovic, C. Structural and Mechanical Properties of Supramolecular Polyethylenes. *Macromolecules* **2018**, *51*, 2630−2640.
(65) Yan, L.; Haußler, M.; Bauer, J.; Mecking, S.; Winey, K. I. Monodisperse and Telechelic Polyethylenes Form Extended Chain Crystals with Ionic Layers. *Macromolecules* **2019**, *52*, 4949−4956.
(66) Bell, T. D. M.; Bhosale, S. V.; Forsyth, C. M.; Hayne, D.; Ghiggino, K. P.; Hutchison, J. A.; Jani, C. H.; Langford, S. J.; Lee, M. A.-P.; Woodward, C. P. Melt-Induced Fluorescent Signature in a Simple Naphthalenediimide. *Chem. Commun.* **2010**, *46*, 4881−4883.
(67) Knothe, G.; Dunn, R. O. A Comprehensive Evaluation of the Melting Points of Fatty Acids and Esters Determined by Differential Scanning Calorimetry. *J. Am. Oil Chem. Soc.* **2009**, *86*, 843−856.
(68) Haraldsson, G. Separation of Saturated/Unsaturated Fatty Acids. *J. Am. Oil Chem. Soc.* **1984**, *61*, 219−222.
(69) Miao, X.; Chen, C.; Zhou, J.; Deng, W. Influence of Hydrogen Bonds and Double Bonds on the Alkane and Alkene Derivatives Self-Assembled Monolayers on HOPG Surface: STM Observation and Computer Simulation. *Appl. Surf. Sci.* **2010**, *256*, 4647−4655.
(70) Nečas, D.; Klapetek, P. Gwyddion: An Open-Source Software for SPM Data Analysis. *Open Phys.* **2012**, *10*, 181−188.
(71) Horcas, I.; Fernández, R.; Gómez-Rodríguez, J. M.; Colchero, J.; Gómez-Herrero, J.; Baro, A. M. WSXM : A Software for Scanning Probe Microscopy and a Tool for Nanotechnology. *Rev. Sci. Instrum.* **2007**, *78*, 013705.

https://dx.doi.org/10.1021/acsnano.0c06274
ACS Nano 2020, 14, 13865−13875